Redox Reactions in Strontium Iron Phosphates: Synthesis, Structures, and Characterization of $Sr_9Fe(PO_4)_7$ and $Sr_9FeD(PO_4)_7$

Alexei A. Belik,*[,†,‡,§] Fujio Izumi,[‡] Masaki Azuma,[§,⊥] Takashi Kamiyama,[#] Kenichi Oikawa,[#,@] Konstantin V. Pokholok,[+] Bogdan I. Lazoryak,[+] and Mikio Takano[§]

International Center for Young Scientists (ICYS) and Advanced Materials Laboratory (AML), National Institute for Materials Science (NIMS), 1-1 Namiki, Tsukuba, Ibaraki 305-0044, Japan, Institute for Chemical Research, Kyoto University, Uji, Kyoto-fu 611-0011, Japan, PRESTO, Japan Science and Technology Agency (JST), Kawaguchi, Saitama 332-0012, Japan, Institute of Materials Structure Science, High Energy Accelerator Research Organization, 1-1 Oho, Tsukuba, Ibaraki 305-0801, Japan, and Department of Chemistry, Moscow State University, Leninsky Gory, Moscow 119992, Russia

Received June 7, 2005. Revised Manuscript Received August 12, 2005

Physical and chemical properties of $Sr_9Fe(PO_4)_7$ and $Sr_9FeD(PO_4)_7$ were investigated by Mössbauer, infrared, and Raman spectroscopy, magnetization and dielectric measurements, differential scanning calorimetry, and thermal analysis. $Sr_9Fe(PO_4)_7$ undergoes an antiferroelectric-paraelectric (AFE-PE) phase transition at $T_c = 740$ K. Structure parameters of the AFE phase at 293 K were refined from time-of-flight (TOF) neutron powder diffraction data (space group $C2/c$; $Z = 4$; $a = 14.4971(2)$ Å, $b = 10.6005(13)$ Å, $c = 17.9632(3)$ Å, and $\beta = 112.5053(9)°$), and those of the PE phase at 923 K from synchrotron X-ray powder diffraction data (space group $R3m$; $Z = 3$; $a = 10.70473(13)$ Å and $c = 19.8605(2)$ Å). Parts of Sr atoms and PO_4 tetrahedra are highly disordered in the PE phase. $Sr_9FeD(PO_4)_7$ was prepared by treating $Sr_9Fe(PO_4)_7$ with D_2 at 820 K. The incorporation of D atoms above T_c kept the structure of the high-temperature modification of $Sr_9Fe(PO_4)_7$. Therefore, $Sr_9FeD(PO_4)_7$ is isotypic with the PE phase of $Sr_9Fe(PO_4)_7$. Rietveld refinements from TOF neutron diffraction data and synchrotron XRD data of $Sr_9FeD(PO_4)_7$ (at 293 K) on the basis of space group $R\bar{3}m$ gave lattice parameters $a = 10.67744(13)$ Å and $c = 19.5810(2)$ Å, making it possible to locate D atoms at two positions. Oxidation of $Sr_9FeD(PO_4)_7$ in air above 673 K regenerated $Sr_9Fe(PO_4)_7$. When $Sr_9FeD(PO_4)_7$ was heated above 940 K in the absence of oxygen and when $Sr_9Fe(PO_4)_7$ was treated by 5% H_2 + 95% N_2 above 1100 K, they decomposed to $Sr_2P_2O_7$ and $Sr_{9.333}Fe_{1.167}(PO_4)_7$.

Introduction

Redox reactions proceeding without destroying fundamental structures play important roles in materials science. For example, the stability of the olivine-type structure of $LiMPO_4$ (M = Fe, Ni, and Co)[1] and the NASICON-related structure of $Li_3Fe_2(PO_4)_3$[2] toward extraction/insertion of lithium ions is essential for the application of these materials to cathodes in rechargeable lithium ion batteries. The structure stability is desirable in heterogeneous catalysts, ion-exchange materials, and so on.

Some copper- and iron-containing phosphates, e.g., NASICON-type $Cu_{0.5}Zr_2(PO_4)_2$[3] and whitlockite-type $Ca_{9.5}Cu(PO_4)_7$[4] and $Ca_9Fe(PO_4)_7$,[5,6] react with hydrogen to form $Cu_{0.5}H_{0.5}Zr_2(PO_4)_2$, $Ca_{9.5}CuH_x(PO_4)_7$, and $Ca_9FeH(PO_4)_7$, respectively, and then regenerate in an oxidizing atmosphere. The fundamental structures of these compounds are stable in a certain temperature range, but colors,[3,4,6] electrical conductivities,[6] and some other properties change during redox reactions. These compounds may therefore be potential materials for heterogeneous catalysis,[7] gas sensing,[8] and purification of gas mixtures by removing H_2.[9]

* To whom correspondence should be addressed. Tel: +81 (029) 851-3354 (ext. 8587). Fax: +81 (029) 860-4706. E-mail: Alexei.BELIK@nims.go.jp. International Center for Young Scientists, National Institute for Materials Science, Namiki 1-1, Tsukuba, Ibaraki 305-0044, Japan.
† ICYS.
‡ AML.
§ Kyoto University.
⊥ PRESTO.
Institute of Materials Structure Science.
+ Moscow State University.
@ Present address: Center for Proton Accelerator Facility, Japan Atomic Energy Research Institute, Tokai, Ibaraki 319-1195, Japan.

(1) (a) Nakayama, M.; Goto, S.; Uchimoto, Y.; Wakihara, M.; Kitajima, Y. *Chem. Mater.* **2004**, *16*, 3399. (b) Herle, P. S.; Ellis, B.; Coombs, N.; Nazar, L. F. *Nat. Mater.* **2004**, *3*, 147. (c) Whittingham, M. S. *Chem. Rev.* **2004**, *104*, 4271.
(2) (a) Masquelier, C.; Padhi, A. K.; Nanjundaswamy, K. S.; Goodenough, J. B. *J. Solid State Chem.* **1998**, *135*, 228. (b) Zhu, S.; Zhou, H.; Miyoshi, T.; Hibino, M.; Honma, I.; Ichihara, M. *Adv. Mater.* **2004**, *16*, 2012.
(3) Le Polles, G.; El Jazouli, A.; Olazcuaga, R.; Dance, J. M.; Le Flem, G.; Hagenmuller, P. *Mater. Res. Bull.* **1987**, *22*, 1171.
(4) Lazoryak, B. I.; Khan, N.; Morozov, V. A.; Belik, A. A.; Khasanov, S. S. *J. Solid State Chem.* **1999**, *145*, 345.
(5) Belik, A. A.; Izumi, F.; Stefanovich, S. Yu.; Lazoryak, B. I.; Oikawa, K. *Chem. Mater.* **2002**, *14*, 3937.
(6) Lazoryak, B. I.; Belik, A. A.; Kotov, R. N.; Leonidov, I. A.; Mitberg, E. B.; Karelina, V. V.; Kellerman, D. G.; Stefanovich, S. Yu.; Avetisov, A. K. *Chem. Mater.* **2003**, *15*, 625.
(7) (a) Legrouri, A.; Romdhane, S. S.; Lenzi, J.; Lenzi, M.; Bonel, G. *J. Mater. Sci.* **1996**, *31*, 2469. (b) Benarafa, A.; Kacimi, M.; Coudurier, G.; Ziyad, M. *Appl. Catal. A* **2000**, *196*, 25. (c) Lee, S. J.; Jun, J. H.; Lee, S.-H.; Yoon, K. J.; Lim, T. H.; Nam, S.-W.; Hong, S.-A. *Appl. Catal. A* **2002**, *230*, 61.
(8) Lazoryak, B. I. In *Fundamental Study of New Materials and Processes in the Substance* (in Russian); Moscow State University Press: Moscow, 1994; p 54.
(9) Lazoryak, B. I.; Morozov, V. A.; Zhdanova, A. N. RF Patent 95100507/26, 1995.

10.1021/cm0512169 CCC: $30.25
Published on Web 09/27/2005

Strontium phosphates, $Sr_9R(PO_4)_7$ (R = Sc, Cr, Fe, Ga, In, Y, and Gd−Lu), with a structure closely related to those of β-$Ca_3(PO_4)_2$[10] and $Ca_9Fe(PO_4)_7$, have recently been prepared and characterized.[11,12] An antiferroelectric-paraelectric phase transition at 773 K was found in $Sr_9In(PO_4)_7$.[13] Antiferroelectic phase transitions in inorganic compounds are rarely observed compared to ferroelectric ones.[14] In $Sr_9Fe(PO_4)_7$, redox reactions may occur in the same manner as with $Ca_9Fe(PO_4)_7$. $Sr_9Fe(PO_4)_7$ may also show interesting dielectric properties similar to those of $Sr_9In(PO_4)_7$.

In this work, we have investigated redox reactions in $Sr_9Fe(PO_4)_7$, that is, structural, chemical, and physical properties of $Sr_9Fe(PO_4)_7$ and $Sr_9FeD(PO_4)_7$. Rietveld refinements from time-of-flight (TOF) neutron powder diffraction data of $Sr_9Fe(PO_4)_7$ and $Sr_9FeD(PO_4)_7$ measured at room temperature allowed us to acquire significant information about locations of D atoms in $Sr_9FeD(PO_4)_7$ and structural changes accompanying the redox reactions. The crystal structure of the paraelectric phase for $Sr_9Fe(PO_4)_7$ was also determined from synchrotron X-ray powder diffraction (XRD) data collected at 923 K.

Experimental Section

Synthesis. $Sr_9Fe(PO_4)_7$ was prepared from a mixture of $SrCO_3$ (99.999%), Fe_2O_3 (99.9%), and $NH_4H_2PO_4$ (99.999%) with an amount-of-substance ratio of 9:0.5:7. The mixture was contained in an alumina crucible, heated under air while the temperature was raised very slowly from room temperature (RT) to 900 K, reground, and allowed to react at 1370 K for 120 h with three intermediated grindings. $Sr_9FeD(PO_4)_7$ was synthesized by treating $Sr_9Fe(PO_4)_7$ with 20% D_2 + 80% Ar at 820 K for 48 h in a closed setup. $Sr_9Fe(PO_4)_7$ was light-red while $Sr_9FeD(PO_4)_7$ was white. A very small amount of an impurity, α-$Sr_2P_2O_7$, was detected by X-ray powder diffraction in the sample of $Sr_9FeD(PO_4)_7$ whereas that of $Sr_9Fe(PO_4)_7$ was monophasic. $Sr_9FeH(PO_4)_7$ was prepared by treating $Sr_9Fe(PO_4)_7$ at 820 K in a flowing mixture of 20% H_2 + 80% Ar.

Measurements of Physical Properties. We recorded ^{57}Fe Mössbauer spectra of $Sr_9Fe(PO_4)_7$, $Sr_9FeH(PO_4)_7$, and $Sr_9FeD(PO_4)_7$ using a constant-acceleration Mössbauer spectrometer coupled with a multichannel analyzer with a ^{57}Co/Rh source kept at RT. All the isomer shifts, δ, were determined with reference to α-Fe. Lorentzian functions were fit to the resulting spectra. $Sr_9Fe(PO_4)_7$ and $Sr_9FeH(PO_4)_7$ were enriched with ^{57}Fe up to 14%.

Magnetic susceptibilities, $\chi = \mathbf{M}/\mathbf{H}$, of $Sr_9Fe(PO_4)_7$ and $Sr_9FeD(PO_4)_7$ were measured on a dc SQUID magnetometer (Quantum Design, MPMS XL) between 2 and 300 K in an applied field of 100 Oe (1 Oe = $(10^3/4\pi)$ Am^{-1}) under both zero-field-cooled (ZFC) and field-cooled (FC) conditions. Isothermal magnetization curves were recorded at 1.8 K in applied fields from 0 to 70 kOe.

Specific heats, $C_p(T)$, of $Sr_9Fe(PO_4)_7$ were measured between 0.4 and 55 K (on cooling) at a zero magnetic field by a pulse relaxation method on a Quantum Design PPMS calorimeter.

Infrared (IR) spectra of $Sr_9Fe(PO_4)_7$, $Sr_9FeH(PO_4)_7$, and $Sr_9FeD(PO_4)_7$ were recorded on a Nicolet Magna-750 Fourier spectrometer in a wavenumber ($\tilde{\nu}$) range of 4000 to 460 cm^{-1} using the KBr pellet technique. Unpolarized Raman spectra of $Sr_9Fe(PO_4)_7$ and $Sr_9FeD(PO_4)_7$ were collected at RT with a micro Raman spectrometer (Horiba Jobin-Yvon T64000) in back-scattering geometry with a liquid-nitrogen-cooled CCD detector. Raman scattering was excited using an Ar^+−Kr^+ laser at a wavelength of 514.5 nm. A 90× long working distance objective was used to focus the laser beam onto a spot of about 2 μm in diameter. The laser power on the samples was about 2 mW.

To measure the dielectric permittivity (ϵ) of $Sr_9Fe(PO_4)_7$, we used the sample in the form of pellets (ca. 1 mm in length and ca. 5 mm in diameter). They were pelletized by pressing at 200 kgf/cm^2 and sintering at 1370 K for 30 h. Ag paste was put on flat surfaces of the pellets, which were then heated to 923 K to produce metal electrodes. The permittivity was recorded with an LCR meter at electric-field frequencies of 10, 100, and 1000 kHz in a temperature range of 300−1000 K.

Thermal Analysis. The thermal stability of the phosphates was examined on a MAC Science TG-DTA 2000 instrument at a heating rate of 10 K/min. $Sr_9Fe(PO_4)_7$ and $Sr_9FeD(PO_4)_7$ were heated in air and in 5% H_2 + 95% N_2. Differential scanning calorimetry (DSC) curves of $Sr_9Fe(PO_4)_7$ and $Sr_9FeD(PO_4)_7$ were recorded up to 873 K at a heating rate of 10 K/min on a RIGAKU Thermo plus DSC8240 instrument in open and sealed aluminum capsules.

XRD Experiments and Structure Refinements. High-temperature XRD data of $Sr_9Fe(PO_4)_7$ were collected on a RIGAKU RINT 2500 diffractometer (2θ range of 8−100°, a step width of 0.02°, and a counting time of 1 s/step).

Synchrotron XRD data were measured at RT for $Sr_9FeD(PO_4)_7$ and at RT and 923 K for $Sr_9Fe(PO_4)_7$ on a Debye−Scherrer type powder diffractometer BL02B2 at SPring-8.[15] The samples were contained in glass (or quartz) capillary tubes with an inner diameter of 0.2 mm and rotated during the measurements. The synchrotron XRD data were collected for 15−20 min at a wavelength of ca. 0.776 Å (see Table 1) in a 2θ range from 1° to 74° with a step interval of 0.01°.

The XRD data were analyzed by the Rietveld method with RIETAN-2000.[16] Coefficients for analytical approximation to atomic scattering factors for Sr, Fe, P, and O were taken from ref 17. The split pseudo-Voigt function of Toraya[18] was used as a profile function. The background was represented by a composite background function, i.e., an 11th-order Legendre polynomial multiplied by a set of numerical values to approximate the background. Isotropic atomic displacement parameters, U, with the isotropic Debye−Waller factor represented as $\exp((-8\pi^2 U \sin^2\theta)/\lambda^2)$ were assigned to all the sites. For the second phase, α-$Sr_2P_2O_7$, in the sample of $Sr_9FeD(PO_4)_7$, we refined only a scale factor and lattice parameters (a, b, and c), fixing its structure parameters.[19] The mass percentage of α-$Sr_2P_2O_7$ in $Sr_9FeD(PO_4)_7$ was calculated at 0.2% from the refined scale factors.

Time-of-Flight (TOF) Neutron Powder Diffraction Experiments and Structure Refinements. TOF neutron powder diffraction data of $Sr_9Fe(PO_4)_7$ and $Sr_9FeD(PO_4)_7$ were measured at RT

(10) (a) Dickens, B.; Schroeder, L. W.; Brown, W. E. *J. Solid State Chem.* **1974**, *10*, 232. (b) Yashima, M.; Sakai, A.; Kamiyama, T.; Hoshikawa, A. *J. Solid State Chem.* **2003**, *175*, 272.
(11) Belik, A. A.; Izumi, F.; Ikeda, T.; Okui, M.; Malakho, A. P.; Morozov, V. A.; Lazoryak, B. I. *J. Solid State Chem.* **2002**, *168*, 237.
(12) Belik, A. A.; Azuma, M.; Takano, M. *Solid State Ionics* **2004**, *172*, 533.
(13) Stefanovich, S. Yu.; Belik, A. A.; Azuma, M.; Takano, M.; Baryshnikova, O. V.; Morozov, V. A.; Lazoryak, B. I.; Lebedev, O. I.; Van Tendeloo, G. *Phys. Rev. B* **2004**, *70*, 172103.
(14) (a) Yasuda, N.; Okamoto, M.; Shimizu, H.; Fujimoto, S.; Yoshino, K.; Inuishi, Y. *Phys. Rev. Lett.* **1978**, *41*, 1311. (b) Ranjan, R.; Pandey, D.; Lalla, N. P. *Phys. Rev. Lett.* **2000**, *84*, 3726.
(15) Nishibori, E.; Takata, M.; Kato, K.; Sakata, M.; Kubota, Y.; Aoyagi, S.; Kuroiwa, Y.; Yamakata, M.; Ikeda, N. *Nucl. Instrum. Methods Phys. Res. Sect. A* **2001**, *467−468*, 1045.
(16) Izumi, F.; Ikeda, T. *Mater. Sci. Forum* **2000**, *321−324*, 198.
(17) *International Tables for Crystallography*, Vol. C, 2nd ed.; Wilson, A. J. C., Prince, E., Eds.; Kluwer: Dordrecht, The Netherlands, 1999; pp 572−574.
(18) Toraya, H. *J. Appl. Crystallogr.* **1990**, *23*, 485.
(19) Barbier, J.; Echard, J. P. *Acta Crystallogr., Sect. C* **1998**, *54*, IUC9800070.

Table 1. Conditions of the Diffraction Experiments and Parts of Refinement Results for $Sr_9Fe(PO_4)_7$ and $Sr_9FeD(PO_4)_7$

	$Sr_9Fe(PO_4)_7$	$Sr_9Fe(PO_4)_7$	$Sr_9FeD(PO_4)_7$	$Sr_9FeD(PO_4)_7$
temperature (K)	293	923	293	293
beam	Neutron	X-ray	Neutron	X-ray
wavelength (Å)		0.77578		0.77600
2θ range; step (deg)		4−70; 0.01		4−74; 0.01
d range (Å)	0.57−5.0		0.5−5.0	
number of data points	3795	6601	3970	7001
space group	$C2/c$ (No. 15)	$R\bar{3}m$ (No. 166)	$R\bar{3}m$ (No. 166)	$R\bar{3}m$ (No. 166)
Z	4	3	3	3
lattice parameters				
a (Å)	14.4971(2)	10.70473(13)	10.67744(13)	10.67616(6)
b (Å)	10.60046(13)			
c (Å)	17.9632(3)	19.8605(2)	19.5810(2)	19.57536(9)
β (deg)	112.5053(9)			
V (Å^3)	2550.28(7)	1970.93(4)	1933.30(4)	1932.28(2)
number of Bragg reflections	7194	853	1991	958
variables:				
background; profiles	15; 18	12; 7	15; 18	12; 10
structure	99	31	58	30
others	2	2	3	6
R_{wp} (%); R_p (%)	2.70; 2.24	2.40; 1.77	2.79; 2.29	3.34; 2.46
R_B (%); R_F (%)	0.80; 0.70	2.86; 1.95	1.28; 1.14	2.09; 1.59
$S = R_{wp}/R_e$	1.34	0.92	1.53	1.77

on the powder diffractometer Vega[20] ($\Delta d/d \approx 2 \times 10^{-3}$; d: spacing of lattice planes) at the pulsed spallation neutron facility KENS. About 8.0 g of each sample was contained in a V holder (diameter: 9.2 mm), which was slowly rotated during the measurement. An array of 160 position-sensitive detectors (PSDs) installed in a backward bank with a 2θ range from 150° to 170° was used to measure the intensity data. Incident neutron spectra were monitored with a ^{3}He monitor counter. Differences in efficiency between the PSDs and the monitor counter were corrected with intensity data resulting from a separate measurement of incoherent scattering from V.

Neutron powder diffraction data in d ranges from 0.57 to 5.0 Å for $Sr_9Fe(PO_4)_7$ and from 0.5 to 5.0 Å for $Sr_9FeD(PO_4)_7$ were analyzed by the Rietveld method with RIETAN-TN.[21] A composite background function, i.e., a 14th-order Legendre polynomial multiplied by a smoothed incident spectrum, was fit to the background. Bound coherent scattering lengths, b_c, used for the structure refinements were 7.02 fm (Sr), 9.45 fm (Fe), 5.13 fm (P), 5.803 fm (O), and 6.671 fm (D).[22]

Results

Characterization of $Sr_9Fe(PO_4)_7$ and $Sr_9FeD(PO_4)_7$. Figure 1 presents the Mössbauer spectra of $Sr_9Fe(PO_4)_7$ and $Sr_9FeD(PO_4)_7$. $Sr_9Fe(PO_4)_7$ demonstrated a very broad peak with $\delta = 0.52$ mm/s characteristic of iron(III). A very broad peak was also observed in the Mössbauer spectrum of $Ca_9Fe(PO_4)_7$.[6,23] The broad peak is attributed to relaxation effects. $Sr_9FeD(PO_4)_7$ showed a doublet with $\delta = 1.11$ mm/s, which provides corroborative evidence that Fe in $Sr_9FeD(PO_4)_7$ has the oxidation state of +2. The doublet in $Sr_9FeD(PO_4)_7$ was broadened with a full-width at half-maximum, Γ, of 0.32 mm/s and a quadrupole splitting, Δ_Q, of 1.24 mm/s. The Mössbauer spectra of $Sr_9FeD(PO_4)_7$ and $Sr_9FeH(PO_4)_7$ were very similar to each other (see Supporting Information).

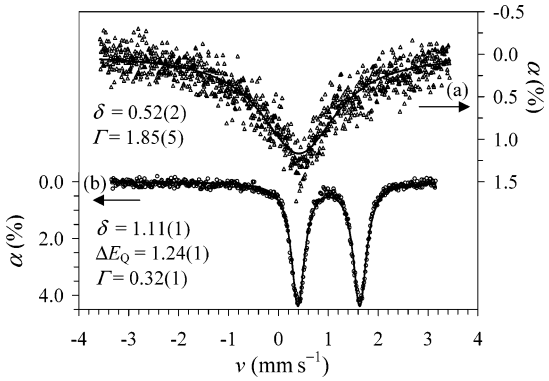

Figure 1. Mössbauer spectra of (a) $Sr_9Fe(PO_4)_7$ and (b) $Sr_9FeD(PO_4)_7$ at RT. v: velocity; α: absorption. Triangles and circles are experimental data, to which solid lines are fit. Hyperfine parameters refined by least-squares fitting are included in the figure, where δ is the isomer shift, ΔE_Q is the quadrupole splitting, and Γ is the full-width at half-maximum with a unit of mm s^{-1}.

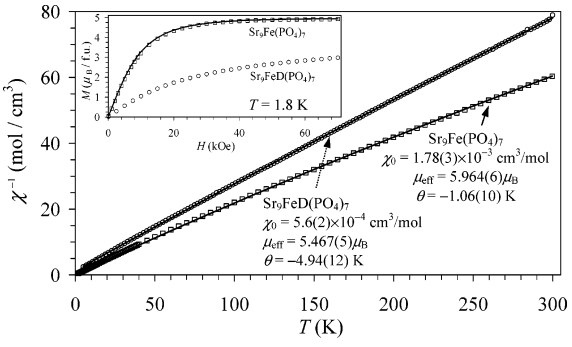

Figure 2. Inverse magnetic susceptibility, χ^{-1}, vs temperature for $Sr_9Fe(PO_4)_7$ and $Sr_9FeD(PO_4)_7$. Solid lines show Curie−Weiss equations (eq 1) fit with the parameters given in the figure. The inset illustrates the isothermal magnetization curves, M vs H, at $T = 1.8$ K. The solid line for the M vs H curve of $Sr_9Fe(PO_4)_7$ is the Brillouin function with $S = 5/2$ and $g = 1.98$.

Figure 2 displays plots of χ^{-1} (FC curves) versus temperature, T, for $Sr_9Fe(PO_4)_7$ and $Sr_9FeD(PO_4)_7$. No noticeable difference was found between the curves measured under the ZFC and FC conditions. The χ^{-1} versus T curves obeyed the modified Curie−Weiss law in the whole temperature range

(20) Kamiyama, T.; Oikawa, K.; Tsuchiya, N.; Osawa, M.; Asano, H.; Watanabe, N.; Furusaka, M.; Satoh, S.; Fujikawa, I.; Ishigaki, T.; Izumi, F. *Physica B* **1995**, *213*−*214*, 875.
(21) Ohta, T.; Izumi, F.; Oikawa, K.; Kamiyama, T. *Physica B* **1997**, *234*−*236*, 1093.
(22) Sears, V. F. *International Tables for Crystallography*, 2nd ed.; Kluwer: Dordrecht, The Netherlands, 1999; Vol. C, pp 440−450.
(23) Lazoryak, B. I.; Morozov, V. A.; Safonov, M. S.; Khasanov, S. S. *Mater. Res. Bull.* **1995**, *30*, 1269.

$$\chi(T) = \chi_0 + \mu_{\text{eff}}{}^2 N(3k_B(T-\theta))^{-1} \quad (1)$$

where χ_0 is the temperature-independent term, μ_{eff} is the effective magnetic moment, N is Avogadro's number, k_B is Boltzmann's constant, and θ is the Weiss constant. The three parameters, χ_0, μ_{eff}, and θ, obtained by curve-fitting are given in Figure 2. $Sr_9Fe(PO_4)_7$ and $Sr_9FeD(PO_4)_7$ are paramagnetic over the whole range of temperature. In $Sr_9Fe(PO_4)_7$, μ_{eff} ($=5.96\mu_B$) was very close to that expected for a free Fe^{3+} ion ($\mu_{\text{eff}} = 5.91\mu_B$). In $Sr_9FeD(PO_4)_7$, μ_{eff} ($=5.47\mu_B$) was within the range usually observed for Fe^{2+} ions.[24]

The magnetization curve, M vs H, for $Sr_9Fe(PO_4)_7$ peaked out above about 50 kOe to give an M value of 4.94 μ_B/f.u. expected for the Fe^{3+} ion (high spin), as illustrated in the inset of Figure 2. The M versus H curve agreed very well with the Brillouin function[24] with $S = {}^5/_2$ and $g = 1.98$ (at $T = 1.8$ K). The M versus H curve for $Sr_9FeD(PO_4)_7$ did not peak out at 1.8 K and 70 kOe ($M = 2.98$ μ_B/f.u. at 70 kOe and 1.8 K).

The C_p versus T curve for $Sr_9Fe(PO_4)_7$ increased rapidly below about 2 K, probably owing to long-range magnetic ordering with a phase transition temperature below 0.4 K (see Supporting Information).

The IR spectrum of $Sr_9FeD(PO_4)_7$ (Figure 3) showed a very weak and broad absorption band due to O−D stretching in a $\tilde{\nu}$ range from 2630 to 1900 cm^{-1}, a very weak O−D stretching band at 1770 cm^{-1}, and strong P−O stretching and O−P−O bending bands in a $\tilde{\nu}$ range from 1700 to 460 cm^{-1}. The IR spectrum of $Sr_9FeH(PO_4)_7$ (Figure 3b) exhibited a broad and weak absorption band assigned to an O−H stretching vibration in a $\tilde{\nu}$ range between 3500 and 2530 cm^{-1} and weak O−H stretching bands at 2450 and 2360 cm^{-1} in addition to P−O stretching and O−P−O bending bands. The wavenumbers of 2630−1900 and 1770 cm^{-1} in $Sr_9FeD(PO_4)_7$ and those of 3500−2530 and 2450 cm^{-1} in $Sr_9FeH(PO_4)_7$ are consistent with the $\tilde{\nu}$ ratio expected for deuteroxyl and hydroxyl groups in the simple harmonic approximation: $\tilde{\nu}(O-H)/\tilde{\nu}(O-D) = 1.37$.[25] Hence, the bands at 1770 and 2450 (2360) cm^{-1} are assigned to O−D and O−H stretching vibrations, respectively.

The IR spectra of $Sr_9FeD(PO_4)_7$ and $Sr_9FeH(PO_4)_7$ were very similar to each other in the $\tilde{\nu}$ range of the P−O stretching and O−P−O bending bands (see Supporting Information). On the other hand, the IR and Raman spectra of $Sr_9FeD(PO_4)_7$ differed considerably from those of $Sr_9Fe(PO_4)_7$, which suggests that the local symmetry of PO_4 groups in $Sr_9FeD(PO_4)_7$ differ from that in $Sr_9Fe(PO_4)_7$.

Figure 4 depicts the dependence of permittivity on temperature in $Sr_9Fe(PO_4)_7$ at 0.1 and 1 MHz. A clear anomaly was observed at about 740 K. The broad maximum on the ϵ versus T curves in $Sr_9Fe(PO_4)_7$ was less pronounced than that in $Sr_9In(PO_4)_7$.[12] Nevertheless, the dielectric data suggest that $Sr_9Fe(PO_4)_7$ and $Sr_9In(PO_4)_7$ undergo the same type of antiferroelectric-paraelectric transitions. Whereas no anomaly was found in the DTA curve of $Sr_9Fe(PO_4)_7$, a steplike anomaly was detected at 740 K in its DSC curves (inset of Figure 4).

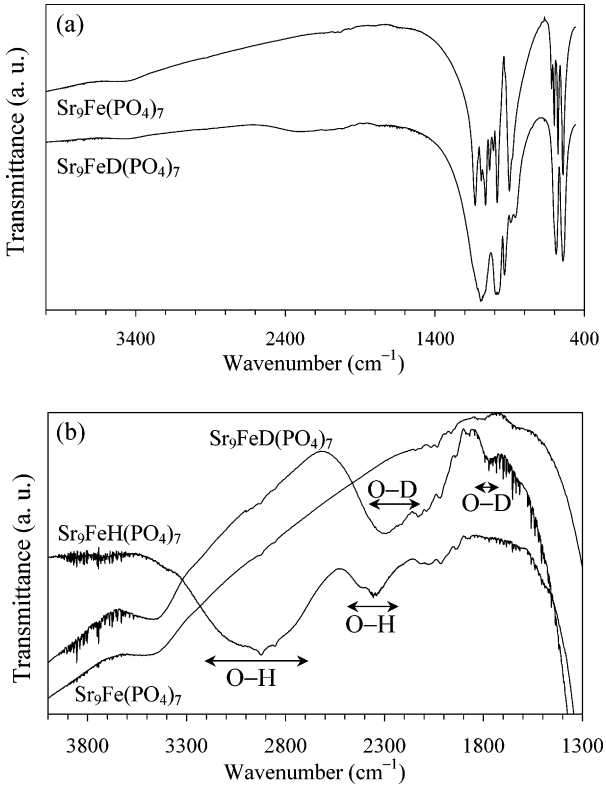

Figure 3. IR spectra in wavenumber $\tilde{\nu}$ regions (a) from 4000 to 400 cm^{-1} for $Sr_9Fe(PO_4)_7$ and $Sr_9FeD(PO_4)_7$ and (b) from 4000 to 1300 cm^{-1} for $Sr_9Fe(PO_4)_7$, $Sr_9FeH(PO_4)_7$, and $Sr_9FeD(PO_4)_7$.

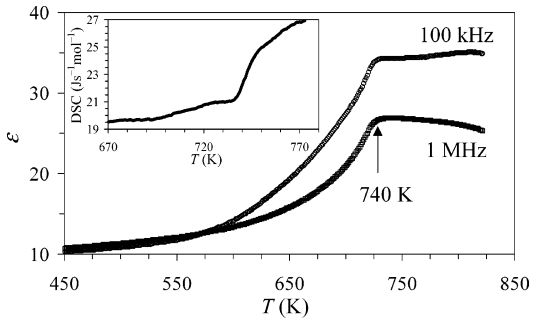

Figure 4. Dependence of the dielectric constant on temperature in $Sr_9Fe(PO_4)_7$ at 100 kHz and 1 MHz during cooling. The phase-transition temperature is marked with an arrow. The inset gives the DSC curve of $Sr_9Fe(PO_4)_7$ on heating near the phase-transition temperature.

Redox Reactions and Thermal Stability of $Sr_9Fe(PO_4)_7$ and $Sr_9FeD(PO_4)_7$. As described above, $Sr_9FeD(PO_4)_7$ was the exclusive product of reducing $Sr_9Fe(PO_4)_7$ except for 0.2 mass % of α-$Sr_2P_2O_7$; that is too small to change significantly the stoichiometry of $Sr_9FeD(PO_4)_7$. This finding, coupled with the results of Mössbauer and IR spectroscopy, and the magnetization measurements, supports the idea that the oxidation state of Fe changes from +3 to +2 on the reduction of $Sr_9Fe(PO_4)_7$ with D_2 at 820 K:

$$2Sr_9Fe^{3+}(PO_4)_7 + D_2 = 2Sr_9Fe^{2+}D(PO_4)_7 \quad (2)$$

When the reduction is complete, the limiting formula of $Sr_9FeD(PO_4)_7$ is reached.

(24) Kittel, C. *Introduction to Solid State Physics*, 6th ed.; Wiley & Sons: New York, 1986; p 406.
(25) Nakamoto, K. *Infrared Spectra of Inorganic and Coordination Compounds*; Wiley: New York, 1963.

Heating $Sr_9FeD(PO_4)_7$ in air up to 1270 K is believed to change the oxidation state of Fe from +2 to +3 with releasing D_2O:

$$4Sr_9Fe^{2+}D(PO_4)_7 + O_2 = 4Sr_9Fe^{3+}(PO_4)_7 + 2D_2O \quad (3)$$

The light-red product of the oxidation was $Sr_9Fe(PO_4)_7$, whose XRD pattern, lattice parameters, and *M* versus *H* curve at 1.8 K were very similar to those of as-synthesized $Sr_9Fe(PO_4)_7$. The observed total mass loss of 0.12% during the TG experiment in air was close to a mass loss of 0.13% calculated with eq 3. However, no clear anomalies were observed in the DTA or DSC curves. This fact supports the idea that the oxidation is slow, proceeding in a relatively wide temperature range.

To determine when the oxidation starts, we measured XRD patterns and *M* versus *H* curves at 1.8 K for $Sr_9FeD(PO_4)_7$ heated to 473, 573, 673, 773, 873, and 973 K in air and then kept at each temperature for 1 h. A monoclinic phase characteristic of the oxidized samples (see below) appeared at 673 K, and the *M* versus *H* curve of this sample reached 4.67 μ_B/f.u. at 70 kOe. Therefore, $Sr_9FeD(PO_4)_7$ was almost completely oxidized at 673 K (see Supporting Information). For the oxidation at 573 K and below, the samples had trigonal symmetry characteristic of as-synthesized $Sr_9FeD(PO_4)_7$. However, their *M* versus *H* curves were different from that of as-synthesized $Sr_9FeD(PO_4)_7$. This fact shows that the samples were partially oxidized below 673 K.

When $Sr_9FeD(PO_4)_7$ was heated from about 940 to 1270 K in the absence of oxygen, the mass loss was 0.70%. The product was white and contained α-$Sr_2P_2O_7$, whose mass percentage was calculated at 10.8% from the scale factor refined in the Rietveld analysis, and a phase similar to $Sr_{9+x}Fe_{1.5-x}(PO_4)_7$.[26] The complete thermal decomposition of $Sr_9FeD(PO_4)_7$ can be formulated as

$$14Sr_9Fe^{2+}D(PO_4)_7 = 12Sr_{9.333}Fe^{2+}_{1.167}(PO_4)_7 + 7Sr_2P_2O_7 + 7D_2O \quad (4)$$

According to eq 4, the mass loss is calculated at 0.66%, and the mass percentage of $Sr_2P_2O_7$ is 11.6%. Note that the solid solutions of $Sr_{9+x}Fe_{1.5-x}(PO_4)_7$ are formed in the compositional range of about $0 \le x \le 0.32$[26] and that the composition of $Sr_{9.333}Fe_{1.167}(PO_4)_7$ corresponds to $x = {}^1/_3$, lying on the boundary of the solid solutions $Sr_{9+x}Fe_{1.5-x}(PO_4)_7$.

When $Sr_9Fe(PO_4)_7$ was heated in the mixture of 5% H_2 and 95% N_2 at the rate of 10 K/min, the mass loss was 0.62% between 1100 and 1270 K. The product was also white and contained $Sr_2P_2O_7$ (mass percentage 9.9%) and $Sr_{9+x}Fe_{1.5-x}(PO_4)_7$. Therefore, when reaction 2 is incomplete at a high temperature, $Sr_9Fe(PO_4)_7$ directly decomposes according to the following reaction

$$14Sr_9Fe^{3+}(PO_4)_7 + 7H_2 = 12Sr_{9.333}Fe^{2+}_{1.167}(PO_4)_7 + 7Sr_2P_2O_7 + 7H_2O \quad (5)$$

Structure Refinement of the Room-Temperature Phase of $Sr_9Fe(PO_4)_7$. Indexing Bragg reflections in the synchrotron X-ray and TOF neutron powder diffraction data of $Sr_9Fe(PO_4)_7$ revealed it to crystallize in the monoclinic system with lattice parameters of $a = 14.4971(2)$ Å, $b = 10.60046(13)$ Å, $c = 17.9632(3)$ Å, and $\beta = 112.5053(9)°$. Reflection conditions derived from the indexed reflections were $h + k = 2n$ for *hkl*, and $h = 2n$ and $l = 2n$ for *h*0*l*, affording possible space groups *C*1*c*1 (No. 9, unique axis *b*, cell choice 1) and *C*12/*c*1 (No. 15, unique axis *b*, cell choice 1).[27] Previous results of second-harmonic generation in $Sr_9R(PO_4)_7$ (R = Sc, Cr, Fe, Ga, and In)[11,13] show $Sr_9Fe(PO_4)_7$ to be centrosymmetric. Hence, $Sr_9Fe(PO_4)_7$ belongs to *C*12/*c*1. From now on, *C*12/*c*1 will be abbreviated to *C*2/*c*.

As initial fractional coordinates in the Rietveld analysis of $Sr_9Fe(PO_4)_7$ from the TOF neutron powder diffraction data, we used those of $Sr_9In(PO_4)_7$ with space group *C*2/*c*.[11] When the Sr4 atom was located at an ideal 4b site (0, ${}^1/_2$, 0; Sr4′) on an inversion center with the occupancy, *g*, of unity, *U*(Sr4′) converged to 0.054(3) Å^2. The Sr4 atom was therefore displaced slightly from the 4b position to a general position (8f). The subsequent Rietveld refinement was rather successful in view of the resulting *R* factors, interatomic distances, bond angles, and *U* parameters, except for *U*(P1) = 0.029(3) Å^2 and *U*(O12) = 0.088(4) Å^2. The large *U*(P1) and *U*(O12) values were also obtained in Rietveld analysis of $Sr_9In(PO_4)_7$ from synchrotron XRD data, reflecting the static disordering of the P1 and O12 atoms.[11]

In the last stage of the Rietveld refinement of $Sr_9Fe(PO_4)_7$, we refined anisotropic atomic displacement parameters, U_{ij}, for the P1 and O12 sites. The isotropic model resulted in $R_{wp} = 3.00\%$ ($S = 1.49$), $R_p = 2.52\%$, $R_B = 1.01\%$, and $R_F = 0.80\%$ while the refinement of U_{ij} for the P1 and O12 sites gave noticeably lower *R* factors: $R_{wp} = 2.70\%$ ($S = 1.34$), $R_p = 2.24\%$, $R_B = 0.80\%$, and $R_F = 0.70\%$. When we introduced a spit-atom model for the P1 and O12 atoms, the P1−O12 distances were 1.41 and 1.74 Å, which are considerably deviated from the typical P−O distance of 1.54 Å in PO_4 groups. Therefore, we adopted not the split-atom model but the anisotropic thermal-vibration one.

Table 1 lists experimental and refinement conditions, lattice parameters, *R* factors, and so forth. Final fractional coordinates and *U* (U_{eq}) parameters for $Sr_9Fe(PO_4)_7$ are listed in Table 2 and selected bond lengths, *l*, calculated with ORFFE[28] in Table 3. Figure 5a displays observed, calculated, and difference TOF neutron diffraction patterns for $Sr_9Fe(PO_4)_7$ at RT.

Structure Refinement of High-Temperature Phase of $Sr_9Fe(PO_4)_7$. The dependence of the lattice parameters on temperature in $Sr_9Fe(PO_4)_7$ was very similar to that in $Sr_9Tb(PO_4)_7$[12] and $Sr_9In(PO_4)_7$.[13] The lattice parameters of $Sr_9Fe(PO_4)_7$ gradually changed with temperature through the phase transition temperature. All weak superlattice reflections with $l = 2n$ and monoclinic splitting of main reflections disappeared in the XRD patterns of $Sr_9Fe(PO_4)_7$ above 740

(26) Belik, A. A.; Lazoryak, B. I.; Pokholok, K. V.; Terekhina, T. P.; Leonidov, I. A.; Mitberg, E. B.; Karelina, V. V.; Kellerman, D. G. *J. Solid State Chem.* **2001**, *162*, 113.

(27) *International Tables for Crystallography*, Vol. A, 5th ed.; Hahn, T., Ed.; Kluwer: Dordrecht, The Netherlands, 2002; p 52.

(28) Busing, W. R.; Martin, K. O.; Levy H. A. *Report ORNL-TM-306*; Oak Ridge National Laboratory: Oak Ridge, TN, 1964.

Table 2. Structure Parameters Determined for $Sr_9Fe(PO_4)_7$ at 293 K from TOF Neutron Diffraction Data

site	Wyckoff position	g^a	x	y	z	10^2U (Å^2)
Sr1	8f	1	−0.2813(3)	0.0060(6)	−0.0865(3)	0.76(10)
Sr2	8f	1	−0.4416(4)	0.7150(5)	−0.1354(3)	0.66(12)
Sr3	8f	1	−0.4452(4)	0.7199(5)	0.3589(3)	1.03(14)
Sr4	8f	1/2	0.0064(7)	0.502(2)	0.0201(5)	0.9(2)
Sr5	8f	1	−0.2345(4)	0.7325(4)	−0.2488(3)	1.19(10)
Fe	4a	1	0	0	0	0.47(6)
P1	4e	1	0	0.4776(14)	1/4	3.16[b]
P2	8f	1	−0.1089(4)	−0.0019(11)	0.2959(3)	0.75(13)
P3	8f	1	−0.1469(6)	0.2589(7)	−0.0545(4)	0.4(2)
P4	8f	1	−0.1503(6)	0.2554(7)	0.4434(4)	0.6(2)
O11	8f	1	−0.0908(4)	0.6140(5)	0.7344(4)	1.42(13)
O12	8f	1	−0.5287(4)	0.9470(6)	−0.3258(4)	9.20[b]
O21	8f	1	−0.7885(3)	0.0028(8)	−0.3052(3)	0.89(12)
O22	8f	1	−0.1004(5)	0.8747(6)	0.2545(4)	0.7(2)
O23	8f	1	−0.0992(5)	0.8868(7)	0.7498(4)	1.0(2)
O24	8f	1	−0.0217(3)	0.0022(8)	0.3808(3)	0.66(11)
O31	8f	1	−0.2421(4)	0.2562(6)	0.1065(4)	0.7(2)
O32	8f	1	−0.3694(5)	0.8570(6)	0.4850(4)	0.3(2)
O33	8f	1	−0.6065(5)	0.6321(7)	−0.0086(4)	0.9(2)
O34	8f	1	−0.4115(5)	0.2008(6)	0.1034(4)	1.0(2)
O41	8f	1	−0.4122(4)	0.2037(6)	−0.3947(4)	0.7(2)
O42	8f	1	−0.3546(5)	0.8562(5)	−0.0070(4)	0.6(2)
O43	8f	1	−0.2422(5)	0.2686(6)	0.6145(4)	0.5(2)
O44	8f	1	−0.6099(5)	0.6260(6)	−0.5118(3)	0.6(2)

[a] Occupancy. [b] $U_{eq} = (1/3)\sum_i\sum_i U_{ij}a_i^*a_i^*\mathbf{a}_i\mathbf{a}_j$.

Table 3. Bond Lengths, *l*, in $Sr_9Fe(PO_4)_7$

bonds	l (Å)	bonds	l (Å)
Sr1−O21	2.514(7)	Sr4−O32	2.48(2)
Sr1−O32	2.579(9)	Sr4−O34	2.60(2)
Sr1−O31	2.588(9)	Sr4−O32a	2.60(2)
Sr1−O43	2.613(9)	Sr4−O42	2.60(2)
Sr1−O42	2.617(9)	Sr4−O41	2.66(2)
Sr1−O12	2.672(7)	Sr4−O42a	2.73(2)
Sr1−O44	2.717(8)	Sr4−O34a	3.02(2)
Sr1−O33	2.729(8)	Sr4−O41a	3.03(2)
Sr1−O11	2.835(8)	Sr4−O12	3.046(12)
		Sr4−Sr4a[a]	0.68(2)
Sr2−O12	2.549(9)	Sr5−O11	2.548(8)
Sr2−O34	2.569(8)	Sr5−O23	2.562(9)
Sr2−O22	2.575(8)	Sr5−O31	2.563(9)
Sr2−O43	2.607(8)	Sr5−O43	2.590(9)
Sr2−O22a	2.618(9)	Sr5−O22	2.616(9)
Sr2−O44	2.630(8)	Sr5−O21	2.637(9)
Sr2−O42	2.631(8)	Sr5−O41	2.657(8)
Sr2−O24	2.644(9)	Sr5−O34	2.986(8)
		Sr5−O21a	3.003(9)
Sr3−O41	2.522(8)	Fe−O44 (×2)	2.027(7)
Sr3−O23	2.544(9)	Fe−O24 (×2)	2.042(6)
Sr3−O32	2.558(8)	Fe−O33 (×2)	2.046(7)
Sr3−O31	2.572(8)	P1−O12 (×2)	1.495(9)
Sr3−O23a	2.600(8)	P1−O11 (×2)	1.572(9)
Sr3−O11	2.617(7)	P2−O23	1.511(10)
Sr3−O24	2.655(9)	P2−O22	1.533(11)
Sr3−O33	2.668(9)	P2−O21	1.558(7)
Sr3−O11a	2.991(8)	P2−O24	1.565(7)
P3−O34	1.497(10)	P4−O43	1.528(9)
P3−O31	1.528(9)	P4−O41	1.544(9)
P3−O33	1.568(9)	P4−O42	1.545(9)
P3−O32	1.572(9)	P4−O44	1.585(9)

[a] Interatomic distance between split positions.

K. This finding also confirms that $Sr_9Fe(PO_4)_7$ undergoes a high-temperature phase transition near 740 K.

Indexing Bragg reflections in the synchrotron XRD data of $Sr_9Fe(PO_4)_7$ at 923 K revealed it to crystallize in the trigonal system with lattice parameters of $a = 10.70473(13)$ Å and $c = 19.8605(2)$ Å. Reflection conditions derived from the indexed reflections were $-h + k + l = 3n$ (hexagonal axes, obverse setting),[27] giving possible space groups of $R3$, $R\bar{3}$, $R32$, $R3m$, and $R\bar{3}m$.

Structure parameters of $Sr_9Fe(PO_4)_7$ were refined on the basis of space group $R\bar{3}m$ using fractional coordinates of $Sr_{9.3}Ni_{1.2}(PO_4)_7$[29] as initial ones in the Rietveld analysis of $Sr_9Fe(PO_4)_7$. A preliminary refinement showed the M4 site, which is 25% occupied by Ni^{2+} and Sr^{2+} ions in $Sr_{9.3}Ni_{1.2}(PO_4)_7$, to be vacant in $Sr_9Fe(PO_4)_7$. Sr atoms at the M3 site (9e: 0, 1/2, 0) and a $P1O_4$ tetrahedron in $Sr_9Fe(PO_4)_7$ were found to be highly disordered in the same manner as with $Sr_{9.3}Ni_{1.2}(PO_4)_7$.[29] In $Sr_9Fe(PO_4)_7$, U parameters were constrained to be equal to each other for two pairs of sites: Sr31 and Sr32 sites and O11 and O12 sites. For the P1 atom, the fractional coordinates and U parameter were refined in different cycles.

Table 1 gives experimental and refinement conditions, lattice parameters, R factors, and so forth. Final fractional coordinates and U parameters for the high-temperature form of $Sr_9Fe(PO_4)_7$ are listed in Table 4 and selected bond lengths in Table 5. Figure 6a displays observed, calculated, and difference synchrotron XRD patterns for $Sr_9Fe(PO_4)_7$ at 923 K.

Structure Refinement of $Sr_9FeD(PO_4)_7$. Reflections in the synchrotron X-ray and TOF neutron powder diffraction data of $Sr_9FeD(PO_4)_7$ at RT could be indexed in the trigonal system with lattice parameters of $a \approx 10.677$ Å and $c \approx 19.581$ Å. Reflection conditions in $Sr_9FeD(PO_4)_7$ were identical to those in the high-temperature phase of $Sr_9Fe(PO_4)_7$. No signal of second-harmonic generation was observed for $Sr_9FeD(PO_4)_7$, which shows it to be centrosymmetric. Structure parameters of $Sr_9FeD(PO_4)_7$ were refined on the basis of space group $R\bar{3}m$. As initial fractional coordinates in the Rietveld analysis of $Sr_9FeD(PO_4)_7$, we used those of $Sr_{9.3}Ni_{1.2}(PO_4)_7$.[29] In $Sr_9FeD(PO_4)_7$, the U parameters of the Sr31 and Sr32 sites were constrained to be equal to

(29) Belik, A. A.; Izumi, F.; Ikeda, T.; Morozov, V. A.; Dilanian, R. A.; Torii, S.; Kopnin, E. M.; Lebedev, O. I.; Van Tendeloo, G.; Lazoryak, B. I. *Chem. Mater.* **2002**, *14*, 4464.

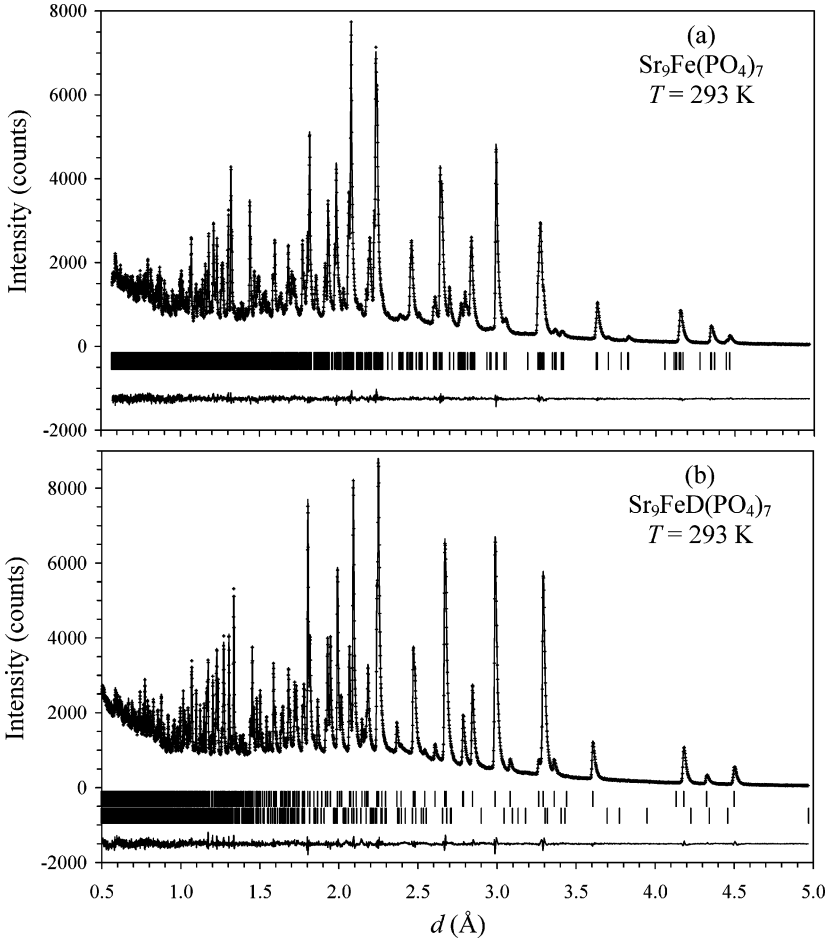

Figure 5. Observed (crosses), calculated (solid line), and difference patterns resulting from the Rietveld analysis of the TOF neutron powder diffraction data for (a) $Sr_9Fe(PO_4)_7$ and (b) $Sr_9FeD(PO_4)_7$ at 293 K. Bragg reflections are indicated by tick marks. The lower tick marks in (b) are given for the impurity phase, α-$Sr_2P_2O_7$.

Table 4. Structure Parameters Determined for $Sr_9Fe(PO_4)_7$ at 923 K from Synchrotron XRD Data

site	Wyckoff position	g	x	y	z	10^2U (Å^2)
Sr1	18h	1	0.18978(3)	$=-x$	0.53655(4)	3.01(3)
Sr31	18h	$^1/_3$	−0.4905(3)	$=-x$	−0.0035(4)	2.42(6)
Sr32	18h	$^1/_6$	−0.5306(4)	$=-x$	0.0145(4)	$=U$(Sr31)
Fe	3a	1	0	0	0	1.68(6)
P1	18h	$^1/_6$	0.0072(11)	$=-x$	0.5079(8)	3.8(2)
P2	18h	1	0.49333(7)	$=-x$	0.39648(10)	1.59(4)
O11	18h	$^1/_3$	−0.6072(9)	$=-x$	0.1175(7)	4.9(4)
O12	36i	$^1/_6$	0.185(2)	0.546(2)	0.1465(9)	$=U$(O11)
O21	18h	1	0.5325(2)	$=-x$	0.6759(2)	2.42(11)
O22	36i	1	0.2670(2)	0.0146(2)	0.23499(12)	1.92(7)
O24	18h	1	0.91144(13)	$=-x$	0.06526(15)	1.56(11)

each other while their occupancies were refined on the assumption that the ideal M3 site is fully occupied.

By trial and error, we located O atoms around the P1 atom in $Sr_9FeD(PO_4)_7$: O11 (6c; $z \approx 0.591$) with g(O11) = $^1/_2$ and O12 (36i; $x \approx 0.973$, $y \approx 0.121$, and $z \approx 0.519$) with g(O12) = $^1/_4$. By trial and error, we also found two positions of D atoms. The first D site proved to lie aside a line connecting O11 with O21 (D1: 18h; $x \approx 0.052$ and $z \approx 0.616$). The second site was near the O12 atom (D2: 36i; $x \approx 0.137$, $y \approx 0.046$, and $z \approx 0.563$). On the assumption that three D atoms are contained in the unit cell of $Sr_9FeD(PO_4)_7$, the following linear constraint was imposed on g(D2): g(D2) = 1/12 − 0.5g(D1). In the last stage of the Rietveld refinement of $Sr_9FeD(PO_4)_7$, we refined U_{ij} parameters for all the atoms except for the disordered atoms Sr31, Sr32,

Table 5. Selected Bond Lengths, l, in $Sr_9Fe(PO_4)_7$ at 923 K

bonds	l (Å)	bonds	l (Å)
Sr1−O22 (×2)	2.591(2)	Sr31−O22 (×2)	2.584(8)
Sr1−O21	2.613(3)	Sr31−O22a (×2)	2.588(7)
Sr1−O24 (×2)	2.659(2)	Sr31−O21 (×2)	2.729(3)
Sr1−O22a (×2)	2.665(2)	Sr31−O21a (×2)	2.966(4)
Sr1−O12 (×2)[a]	2.47(2)	Sr31−O11[a]	2.90(2)
Sr1−O12a (×2)[a]	2.60(2)	Sr31−Sr31a[b]	0.379(8)
Sr1−O11[a]	2.96(2)	Fe−O24 (×6)	2.092(3)
Sr32−O21 (×2)	2.508(4)	P1−O11 (×2)	1.49(2)
Sr32−O22 (×2)	2.605(7)	P1−O12 (×2)	1.59(2)
Sr32−O22a (×2)	2.707(7)		
Sr32−O12 (×2)[a]	2.90(2)	P2−O21	1.515(3)
Sr32−O11[a]	2.49(2)	P2−O22 (×2)	1.533(2)
Sr32−Sr32a[b]	1.273(11)	P2−O24	1.572(3)

[a] Though distances for all the split positions of O11 and O12 are given, only one atom should be included in the first coordination sphere of Sr atoms. [b] Interatomic distance between split positions.

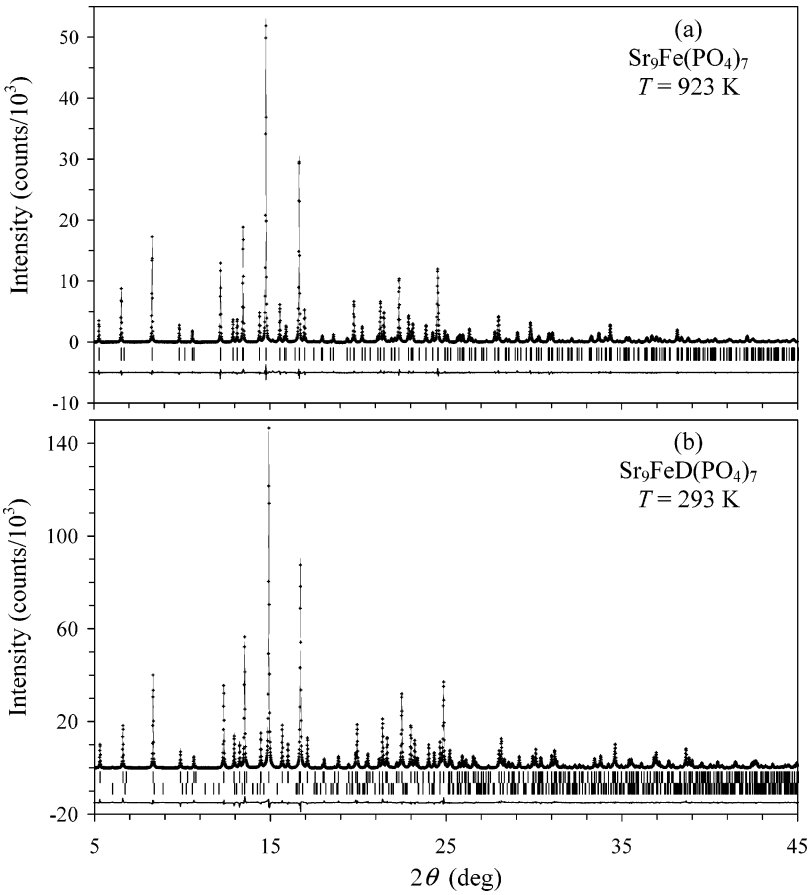

Figure 6. A part (5−45°) of observed, calculated, and difference patterns resulting from the Rietveld analysis of the synchrotron X-ray powder diffraction data for (a) $Sr_9Fe(PO_4)_7$ at 923 K and (b) $Sr_9FeD(PO_4)_7$ at 293 K. Bragg reflections are indicated by tick marks. The lower tick marks in (b) are given for the impurity phase, α-$Sr_2P_2O_7$. Background intensities were subtracted from the observed and calculated XRD data.

Table 6. Structure Parameters Determined for $Sr_9FeD(PO_4)_7$ at 293 K from the TOF Neutron Diffraction Data

site	Wyckoff position	g	x	y	z	10^2U_{eq}[a] or 10^2U (Å^2)
Sr1	18h	1	0.19269(6)	$=-x$	0.53721(6)	0.87
Sr31	18h	0.333(17)	−0.5108(9)	$=-x$	0.0058(5)	0.83(8)[b]
Sr32	18h	0.167[c]	−0.5336(12)	$=-x$	0.0111(6)	$=U$(Sr31)
Fe	3a	1	0	0	0	0.35
P1	6c	1/2	0	0	0.5088(7)	1.7(2)[b]
P2	18h	1	0.49223(9)	$=-x$	0.39638(9)	0.85
O11	6c	1/2	0	0	0.5911(6)	6.88
O12	36i	1/4	0.9731(6)	0.1209(5)	0.5193(2)	3.4(2)[b]
O21	18h	1	0.53336(8)	$=-x$	0.67790(8)	1.81
O22	36i	1	0.26483(10)	0.01217(10)	0.23481(5)	1.30
O24	18h	1	0.90996(7)	$=-x$	0.06806(7)	0.70
D1	18h	0.113(4)	0.0515(9)	$=-x$	0.6156(11)	5.8(9)[b]
D2	36i	0.027[d]	0.137(4)	0.046(5)	0.5633(16)	2(1)[b]

[a] $U_{eq} = (1/3)\sum_i\sum_I U_{ij}a_i^*a_i^*\mathbf{a}_i\mathbf{a}_j$. [b] Isotropic atomic displacement parameters, U. [c] g(Sr32) = 0.5 − g(Sr31). [d] g(D2) = 1/12 − g(D1)/2.

P1, O12, D1, and D2. Note that even O11 is split into a pair of positions, (0, 0, 0.59) and (0, 0, 0.41); U_{ij} could be refined for O11 because these positions are well-separated. When the P1 atom was located at the ideal 3b site (0, 0, 1/2) on an inversion center with g(P1) = 1, U_{33} converged on 0.055(5) Å^2 and was about 4 times as large as U_{11}. The P1 atom was hence displaced slightly from the 3b site to a 6c site along the c axis. For the disordered P1, the U parameter was therefore refined. Attempts to shift the P1 and O11 atoms from a 3-fold rotation axis failed.

Table 1 lists experimental and refinement conditions, lattice parameters, R factors, and so forth. Final fractional coordinates and U (U_{eq}) parameters for $Sr_9FeD(PO_4)_7$ are listed in Table 6 and selected bond lengths in Table 7. U_{ij} parameters are given in Supporting Information. Figure 5b displays observed, calculated, and difference TOF neutron diffraction patterns for $Sr_9FeD(PO_4)_7$.

The $P1O_4$ tetrahedron in $Sr_9FeD(PO_4)_7$ is disordered. The O11 and O12 atoms form D1−O11 and D2−O12 bonds and b_c's for O and D atoms are comparable to each other. It is hard to build a suitable model for Rietveld analysis solely from the neutron diffraction data. Therefore, we refined structure parameters of $Sr_9FeD(PO_4)_7$ from the synchrotron XRD data, where D atoms are almost invisible. Fractional coordinates of $Sr_9FeD(PO_4)_7$ obtained from the TOF neutron diffraction data were used in an initial model for the Rietveld analysis from the synchrotron XRD data. D atoms were not included in the structural model. With the XRD data, we

Table 7. Selected Interatomic Distances (Å) and Angles (deg) in $Sr_9FeD(PO_4)_7$

Sr1−O22(×2)	2.552(1)	Sr31−O22(×2)	2.525(9)
Sr1−O21	2.562(2)	Sr31−O22a(×2)	2.581(8)
Sr1−O24(×2)	2.579(1)	Sr31−O21(×2)	2.700(10)
Sr1−O22a(×2)	2.672(1)	Sr31−O21a(×2)	2.978(11)
Sr1−O12(×2)[b]	2.510(5)	Sr31−O11[b]	3.19(2)
Sr1−O12a(×2)[b]	2.641(5)	Sr31−O12(×2)[b]	3.199(11)
		Sr31−Sr31a[a]	0.46(3)
Sr32−O21(×2)	2.463(11)	Fe−O24 (×6)	2.133(1)
Sr32−O22(×2)	2.610(9)	P1−O11	1.611(16)
Sr32−O22a(×2)	2.643(11)	P1−O12 (×3)	1.557(5)
Sr32−O12(×2)[b]	2.93(2)		
Sr32−O11[b]	2.77(2)	P2−O21	1.529(2)
Sr32−Sr32a[a]	1.32(5)	P2−O22 (×2)	1.540(1)
		P2−O24	1.564(2)
D1−O11	1.066(17)	O21−P2−O22 (×2)	109.31(8)
D1−O21	1.703(18)	O21−P2−O24	111.63(13)
O11−D1−O21	179(2)	O22−P2−O22a	112.98(13)
D2−O12	0.91(3)	O22−P2−O24 (×2)	106.80(8)

[a] Distances between split positions. [b] Distances for all the split positions of O11 and O12 are given.

obtained the same arrangement of the $P1O_4$ tetrahedra as with the neutron diffraction data.

Table 1 lists experimental and refinement conditions, lattice parameters, *R* factors, and so forth. Figure 6b displays observed, calculated, and difference synchrotron XRD patterns for $Sr_9FeD(PO_4)_7$. Final fractional coordinates and *U* parameters for $Sr_9FeD(PO_4)_7$ refined from the synchrotron XRD data are listed in Supporting Information.

Discussion

From the measurements of Mössbauer spectra and magnetization, we confirmed the oxidation states of +3 for Fe atoms in $Sr_9Fe(PO_4)_7$ and +2 for those in $Sr_9FeD(PO_4)_7$. To obtain the additional information on formal oxidation states of Fe, we calculated the bond valence sums, *V*,[30] of the octahedral Fe sites in $Sr_9Fe(PO_4)_7$ and $Sr_9FeD(PO_4)_7$ from the Fe−O bond lengths. The resulting *V* values were 2.82 in $Sr_9Fe(PO_4)_7$ and 2.04 in $Sr_9FeD(PO_4)_7$. These *V* values also support the oxidation states of +3 and +2 for Fe in $Sr_9Fe(PO_4)_7$ and $Sr_9FeD(PO_4)_7$, respectively, confirming the validity of reactions 2 and 3.

The structure refinement from the TOF neutron diffraction data of $Sr_9FeD(PO_4)_7$ and its IR spectrum showed that D atoms occupy the definite sites in the crystal structure of $Sr_9Fe(PO_4)_7$ during the reduction process. The wavenumbers of the O−D stretching bands in $Sr_9FeD(PO_4)_7$ and $Ca_9FeD(PO_4)_7$ are very close to each other.[5] However, the ratio of the intensity of the O−D stretching band over the intensity of the P−O stretching band is much smaller in $Sr_9FeD(PO_4)_7$ than that in $Ca_9FeD(PO_4)_7$. This fact can be explained in terms of that disordering of the $P1O_4$ tetrahedra and O11−D---O21 bonds in $Sr_9FeD(PO_4)_7$ which is reflected on the large atomic displacement parameters of the P1, O11, O12, and D1 atoms. Because parts of Sr atoms and $P1O_4$ tetrahedra are disordered in $Sr_9FeD(PO_4)_7$, the local environment of Fe atoms must also be disordered to some extent (Figure 7b), which results in the broadening of the bands in the Mössbauer spectrum of $Sr_9FeD(PO_4)_7$.

D atoms are localized at two positions: D1 and D2. D1 is involved in a hydrogen bond, O11−D1---O21, whereas D2 is not. The crystal data of $Sr_9FeD(PO_4)_7$ afforded the normal O11−D1---O21 bond lengths and angles and O12−D2 bond length (Table 7).

$Sr_9Fe(PO_4)_7$ at RT crystallizes in space group *C*2/*c*. The Sr4 atoms are disordered between two positions near the center of symmetry. The O11 atom in the $P1O_4$ tetrahedron had normal *U* parameter. On the other hand, the thermal ellipsoid of the O12 atom was elongated toward the Sr4 atom (Figure 7), which is attributed to static disordering of the $P1O_4$ tetrahedron around the O11−O11 edge.

$Sr_9Fe(PO_4)_7$ undergoes a phase transition at 740 K. The high-temperature phase crystallizes in space group $R\bar{3}m$ and is characterized by the highly disordered arrangement of the $P1O_4$ tetrahedron, and Sr31 and Sr32 atoms corresponding to the Sr4 and Sr5 atoms in the low-temperature phase (Figure 7). $Sr_9Fe(PO_4)_7$ was reduced at 820 K (eq 2), i.e., above the phase-transition temperature. The marked disordering remains unchanged on the incorporation of D atoms into the high-temperature phase of $Sr_9Fe(PO_4)_7$. Therefore, $Sr_9FeD(PO_4)_7$ at RT has the same symmetry as the high-temperature phase of $Sr_9Fe(PO_4)_7$. The Sr atoms at the M3 site remain disordered among four positions (Sr31 and Sr32), but orientation of the $P1O_4$ tetrahedra in $Sr_9Fe(PO_4)_7$ at 923 K is slightly different from that in $Sr_9FeD(PO_4)_7$. That is, the O11 and O12 atoms are located off the 3-fold rotation axis in $Sr_9Fe(PO_4)_7$ whereas the O11 atom lies on the 3-fold rotation axis in $Sr_9FeD(PO_4)_7$.

$Ca_9Fe(PO_4)_7$ was reduced at 820 K, which is lower than its phase transition temperature of 890 K.[31] The product of the reduction, $Ca_9FeD(PO_4)_7$, has, therefore, the same symmetry (*R*3*c*) as with the low-temperature phase of $Ca_9Fe(PO_4)_7$.[5] However, the introduction of D atoms into $Ca_9Fe(PO_4)_7$ at high temperatures also keeps the arrangement of the $P1O_4$ tetrahedra in two positions. The $P1O_4$ tetrahedron is believed to become more disordered as the phase transition temperature is approached.[31]

The symmetry of $Sr_9Fe(PO_4)_7$ differs from that of $Sr_9FeD(PO_4)_7$ at RT. However, their structural differences are seen only in the degree of disordering of some structural parts. The fundamental structure of $Sr_9Fe(PO_4)_7$ is, hence, stable toward redox reactions (eqs 2 and 3) and insertion/removal of hydrogen atoms.

In conclusion, we have successfully determined the crystal structures of the antiferroelectric and paraelectric phases for $Sr_9Fe(PO_4)_7$, and $Sr_9FeD(PO_4)_7$, clarifying the structural differences between them. The locations of the D atoms could be unambiguously determined by neutron powder diffraction. The crystal data of the two phosphates have served to put forward the mechanisms of reducing $Sr_9Fe(PO_4)_7$ by D_2 (H_2). The fundamental structure of $Sr_9Fe(PO_4)_7$ has proved to be stable toward redox reactions.

Acknowledgment. We thank the staff of beam line BL02B2 at SPring-8 for technical assistance in the synchrotron X-ray

(30) Brese, R. E.; O'Keeffe, M. *Acta Crystallogr., Sect. B* **1991**, *47*, 192.

(31) Lazoryak, B. I.; Morozov, V. A.; Belik, A. A.; Stefanovich, S. Yu.; Grebenev V. V.; Leonidov, I. A.; Mitberg, E. B.; Davydov, S. A.; Lebedev, O. I.; Van Tendeloo, G. *Solid State Sci.* **2004**, *6*, 185.

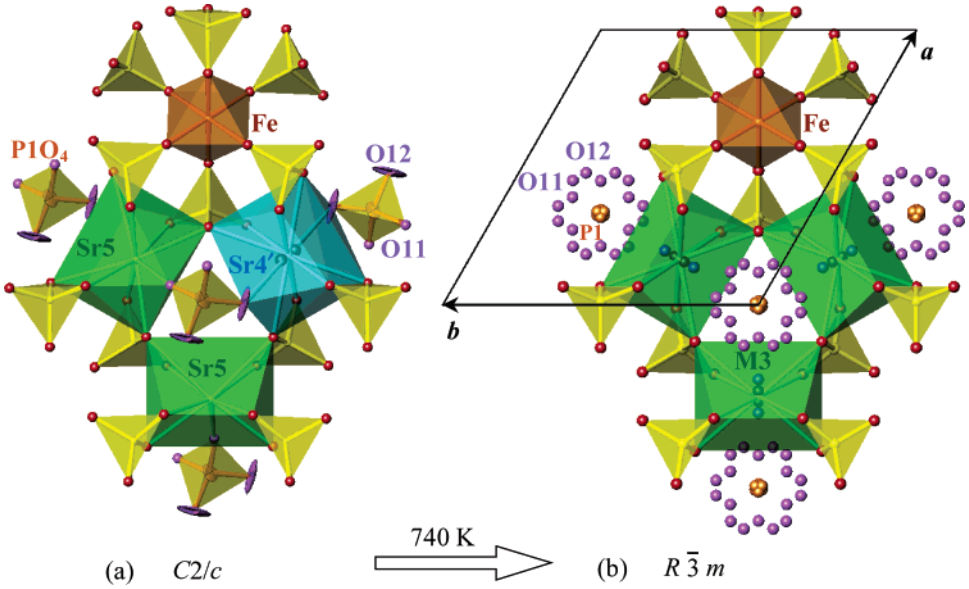

Figure 7. (a) The crystal structure of the low-temperature phase of $Sr_9Fe(PO_4)_7$ viewed along the pseudo 3-fold rotation axis. Polyhedra for the Fe, Sr5, and ideal Sr4′ sites are presented. Circles inside the $Sr4'O_{10}$ polyhedron denote the positions of the Sr4 atoms near the center of symmetry. Thermal ellipsoids are given for the P1 and O12 atoms. (b) The crystal structure of the high-temperature phase of $Sr_9Fe(PO_4)_7$ viewed along the 3-fold rotation axis. Polyhedra for the Fe and ideal M3 sites are presented (the O11 and O12 atoms are not coordinated to M3). Circles inside the $M3O_8$ polyhedron denote the positions of the Sr31 and Sr32 atoms. The disordered P1, O11, and O12 atoms are indicated by circles.

diffraction experiments and Dr. S. Y. Stefanovich for the second-harmonic generation experiments. This work was supported by the Ministry of Education, Culture, Sports, Science and Technology, Japan (Grants-in-Aid No. 12CE2005, COE Research on Elements Science No. 13440111 and No. 14204070, and for 21COE on the Kyoto Alliance for Chemistry) and the Russian Foundation for Basic Research (Grant 04-03-32417). ICYS is supported by Special Coordination Funds for Promoting Science and Technology from MEXT, Japan.

Supporting Information Available: Anisotropic atomic displacement parameters, U_{ij}, in $Sr_9Fe(PO_4)_7$ and $Sr_9FeD(PO_4)_7$ determined from TOF neutron powder diffraction data (Table S1); fractional coordinates and isotropic atomic displacement parameters in $Sr_9FeD(PO_4)_7$ refined from the synchrotron XRD data at 293 K (Table S2); M versus H curves at 1.8 K for $Sr_9FeD(PO_4)_7$ oxidized at different temperatures (Figure S1); the C_p versus T and C_p/T versus T curves for $Sr_9Fe(PO_4)_7$ between 0.4 and 55 K (Figure S2); details of the IR and Raman spectra of $Sr_9Fe(PO_4)_7$ and $Sr_9FeD(PO_4)_7$ (Figure S3); Mössbauer spectra of $Sr_9FeH(PO_4)_7$ and $Sr_9Fe(PO_4)_7$ (Figure S4) (PDF). This material is available free of charge via the Internet at http://pubs.acs.org.

CM0512169